Lab on a Chip

Accepted Manuscript

This is an *Accepted Manuscript*, which has been through the Royal Society of Chemistry peer review process and has been accepted for publication.

Accepted Manuscripts are published online shortly after acceptance, before technical editing, formatting and proof reading. Using this free service, authors can make their results available to the community, in citable form, before we publish the edited article. We will replace this *Accepted Manuscript* with the edited and formatted *Advance Article* as soon as it is available.

You can find more information about *Accepted Manuscripts* in the **Information for Authors**.

ROYAL SOCIETY OF CHEMISTRY

Journal Name

ARTICLE TYPE

Bubble sorting in pinched microchannels for ultrasound contrast agent enrichment[†]

Maarten P. Kok[a], Tim Segers[a], and Michel Versluis[a]

Ultrasound contrast agent (UCA) suspensions contain encapsulated microbubbles with a wide size distribution, with radii between 1 and 10 μm. Medical transducers generally operate at a narrow frequency bandwidth, severely limiting the fraction of bubbles that resonates to the driving ultrasound. Thus, the sensitivity of contrast enhanced ultrasound imaging, molecular imaging with targeted bubbles, and drug delivery with microbubbles can be improved by narrowing down the size distribution of the bubble suspension. Here, we use a low-cost lab-on-a-chip method for the sorting of microbubbles by their size without external actuation, based on a microfluidic separation technique known as pinched flow fractionation (PFF). We show by numerical investigation that the inclusion of particle rotation in the pinched segment is essential for an accurate description of the sorting behavior of particles with sizes close to the pinched segment width. Successful enrichment of a polydisperse contrast agent into a bubble suspension with a narrow size distribution (radius 1.56 ± 0.30 μm) was achieved with a PFF-based microdevice. This sorting technique can be readily parallelized, and may thus lead to an easy-to-use and robust device capable of enriching ultrasound contrast agents, leading to an improvement in the sensitivity of contrast ultrasound imaging.

Introduction

Ultrasound imaging is the most widely used medical imaging modality. It is based on the scattering of sound waves from inhomogeneities in tissue. Contrary to tissue, blood and other liquids in the body scatter ultrasound poorly. Ultrasound contrast agents (UCA) can be added to the blood pool. They consist of stabilized microbubbles, which are excellent ultrasound scatterers, due to the large compressibility of their gas core. The echo produced by a microbubble can be up to a billion times stronger than that of a solid particle of equal size[1]. This strong response allows for the visualization of the blood pool, and can be used to quantify blood perfusion in organs[2]. To facilitate targeted molecular imaging with ultrasound, with a sensitivity up to a single bubble, the shell of the microbubbles allows for the attachment of targeting ligands[3]. The microbubbles can also be loaded with drugs, for use in highly localized delivery of drugs with a low therapeutic index such as chemotherapeutic drugs[4,5], or genes, such as siRNA or mRNA[6–8].

Commercially available UCAs generally consist of encapsulated microbubbles in suspension, with a relatively wide size distribution, with sizes ranging from 1 to 10 μm. Since clinical ultrasound systems operate at a narrow frequency bandwidth, and since the resonant frequency of microbubbles is strongly dependent on the size of the bubbles[1], a significant fraction of the microbubbles will not resonate to the driving ultrasound, while still attenuating the ultrasound. Thus, the sensitivity of contrast-enhanced ultrasound imaging can be improved by narrowing down the size distribution. Furthermore, a highly resonant bubble population also increases the efficiency of drug-loaded agents in releasing their payload. Finally, the use of targeted molecular imaging with ultrasound will highly benefit from the ability to discriminate between bubbles that adhere to a wall and those that freely float, which can be measured by a resonance shift of the adherent monodisperse bubbles[9,10]. Thus, for these reasons it is important to develop a method of obtaining monodisperse ultrasound contrast agents.

There are three main methods to obtain a monodisperse bubble suspension: direct production of monodisperse microbubbles, filtering of polydisperse UCA, or sorting thereof. Recent advances into the production of monodisperse UCA are promising, such as the use of flow-focusing devices to produce highly monodisperse bubble populations as reported by Hettiarachchi et al.[11]. These methods are capable of producing highly monodisperse bubble populations at significant rates[12], however, challenges remain in maintaining the monodispersity for extended periods of

[a] Physics of Fluids Group and MESA+ Institute of Nanotechnology, P.O. Box 217, 7500 AE Enschede, The Netherlands. Fax: +31 53 489 8068; Tel: +31 53 489 2470; E-mail: m.p.kok@utwente.nl

A

B
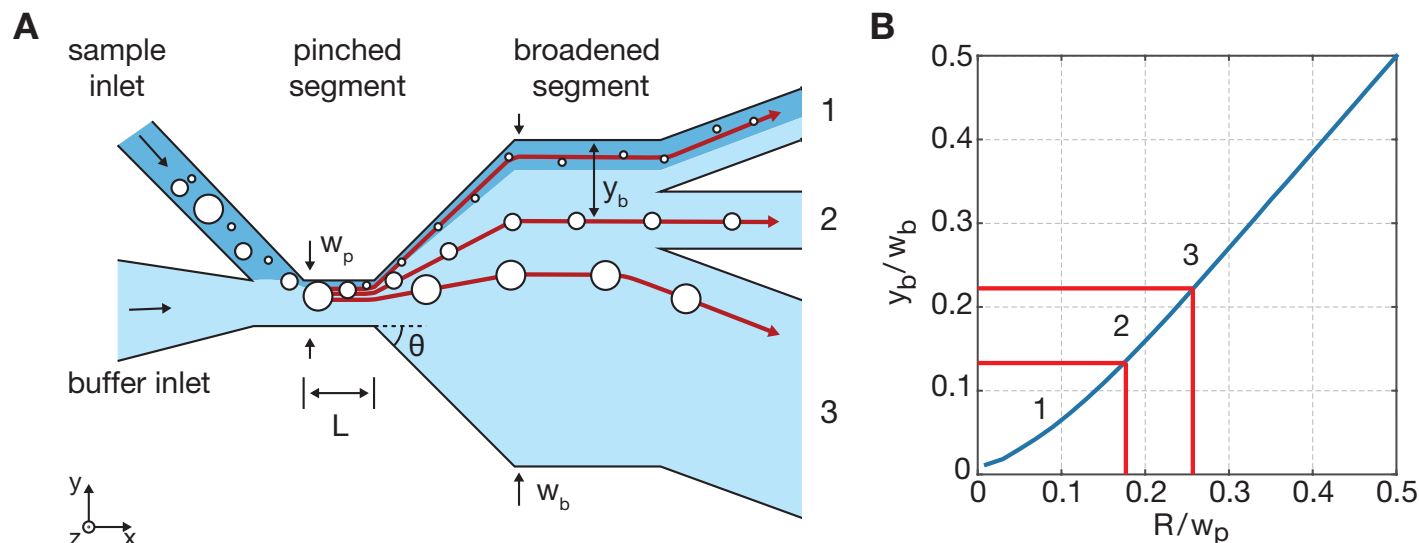
Fig. 1 A) Top view of the microchannel geometry used in pinched flow fractionation. The microbubbles enter the pinched segment and are pinned against the wall by a co-flow. The microbubbles then separate due to the expansion of the channel, to be sorted into exit channels positioned in the broadened segment. The color indicates the inlet of origin for the fluid. B) The expected distance of bubbles from the wall in the broadened segment as a function of bubble radius, based on Eq. 1 combined with an undisturbed velocity profile obtained from 2D COMSOL simulations. Using this result we can design a microdevice geometry to extract microbubbles within a specific size range.

time[13,14]. Mechanical filtration is a widely used technique, where the microbubble suspension is forced through a filter[15], acting as a low-pass filter. However, due to the deformability of the bubbles, bubbles larger than the pore size can also pass the filter. Depending on the amount of pressure used, bubbles are also likely to be fragmented due to being forced through the filter. Furthermore, the filters can become clogged.

Sorting of microbubbles is performed by employing a range of size-dependent forces acting on the microbubbles. Examples of forces used to sort particles in general are the buoyancy force (decantation[16] or centrifugation[17]), optical radiation force[18] and electrical potentials (for charged particles)[19]. Of special interest for the sorting of microbubbles is the acoustic radiation force, which allows for sorting by resonance behavior[20]. Most of these techniques require an actuation force to act on the particles, which can be a complicating factor in the design of practical sorting devices, or requiring optical and acoustical transparency for example.

A novel lab-on-a-chip size-sorting technique for particles, known as pinched flow fractionation (PFF), uses only the properties of laminar flow in microfluidic devices[21]. The method has been successfully applied to the separation by size of solid spheres[21], emulsion droplets[22] and red blood cells[23]. Here we apply the method to the sorting of microbubbles.

The operating principle of PFF is illustrated in Fig. 1A. The microbubbles are introduced into a narrow channel, called the pinched segment, where the bubbles are pinned to the wall by a co-flow from a buffer inlet channel. The co-flow to sample flow rate ratio is typically in the order of 50:1. As the pinched segment expands into a broader segment, the distance from the center of the microbubbles to the wall is extended through microfluidic amplification. Because the centers of the large bubbles are located

further from the wall, they end up closer to the center of the broadened segment. Creating exit channels at different positions thus allows for the sorting of the bubbles into several narrow size distributions.

For infinitesimally small, neutrally buoyant particles (that do not disturb the flow and follow the streamlines), the position in the broadened segment can be found as a function of the position in the pinched segment by tracking the streamlines using mass conservation, which leads to the following equation[24]:

$$\frac{\int_0^H dz \int_{w_b/2-y_b}^{w_b/2} dy \, u_{x,b}(y,z)}{\int_0^H dz \int_{-w_b/2}^{w_b/2} dy \, u_{x,b}(y,z)} = \frac{\int_0^H dz \int_{w_p/2-R}^{w_p/2} dy \, u_{x,p}(y,z)}{\int_0^H dz \int_{-w_p/2}^{w_p/2} dy \, u_{x,p}(y,z)} \quad (1)$$

with H the height of the microchannel, w_b and w_p the width of the broadened and pinched segments, $u_{x,b/p}(y,z)$ the flow profile inside said segments, R the size of the particle and y_b the distance from the wall within the broadened segment.

Vig and Kristensen[25] found good agreement between this model and experimental data for particles up to $(R/w_p = 0.25)$, using a velocity profile obtained from 2D simulations, neglecting the presence of the particles. Figure 1B shows the calculated separation by size. Based on these results, devices can be designed to obtain microbubbles of a specific size range.

Experimental methods
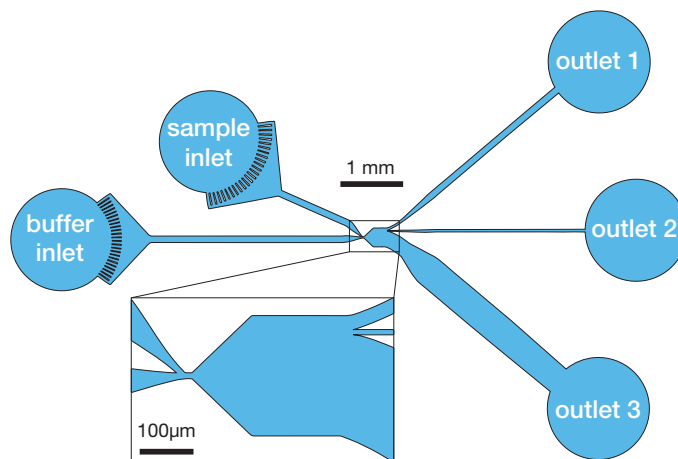
Microfluidic device design

The chip design is displayed in Fig. 2. The design comprises two inlet channels, and three outlet channels, positioned such that only a fraction of bubbles exits through each of the outlets. The two inlet channels merge into the pinched segment, with a width

$w_p = 12$ μm and length $L = 40$ μm. The width is based on the size of the largest bubbles present in the suspension. The pinched segment broadens into the broadened segment with a broadening angle $\theta = 60°$. The broadened segment has a width $w_b = 300$ μm. The broadened segment splits into three outlet channels 600 μm downstream of the pinched segment, with the center outlet located with its center at 20 μm from the side wall, with a width of 10 μm. These positions are designed for the selection for particles with a radius of 1.8 μm. The three outlet channels maintained their width ratios until the outlet ports, to ensure equal outlet hydrodynamic resistance. All the microchannels are 14 μm in height.

Materials and methods

The microfluidic device is fabricated using polydimethylsiloxane (PDMS). PDMS provides a simple and fast prototyping method and is ideal for optical imaging due to its transparency. The molds for the PDMS chips were fabricated using standard soft-lithography techniques[26]: a layer of SU-8 was spin-coated on top of a silicon wafer, UV-exposed through a mask containing the channel features, and developed to be ready for replica molding. The PDMS was mixed in the standard 1 : 10 ratio, degassed, poured over the mold and cured at 65°C for 90 minutes, then cut to size. Prior to bonding, the fluidic ports were punched through the PDMS. The PDMS slab containing the channel features was plasma-bonded to a flat backing slab of PDMS. The backing contains the center outlet port, in order to maintain a constantly rising path for the bubbles, which prevents them from piling up inside the tubing due to buoyancy. The outlets were connected to large diameter tubing to ensure atmospheric pressure at the outlet. The channels were filled with water within ten minutes after bonding to maintain hydrophilicity, while ensuring a strong bond. Teflon tubing was connected to the inlet channels through which the UCA sample and buffer liquid were supplied.

A research-grade contrast agent (Bracco BR-14, Bracco Research Geneva) was used for the characterization of the device. BR-14 microbubbles consist of a perfluorobutane gas core with a stabilizing shell coating of phospholipids, which are reconstituted from powder using purified water (MilliQ, Millipore Corporation, Billerica, MA, USA). The syringe pump controlling the UCA flow was positioned vertically with the needle tip pointing upward at a level several tens of centimeters lower than the sorting chip. With the bubbles being buoyant, the aid of gravity helped to inject the bubble suspension into the sorting chip. The contrast bubbles were infused at a rate of 0.2 μL/min and the liquid co-flow (purified water) had a flow rate of 10 μL/min. These flow rates result in an average flow speed in the pinched segment of approximately 1 m/s. The ratio (1:50) was chosen such that bubbles down to a size of 1 μm are successfully separated. To confirm that the microbubbles act similarly to solid particles (and as such neglect buoyancy and deformability effects), solid particles of different sizes (1.0 and 3.5 μm mean radius, ThermoScientific, Fluoro-Max 35-2 and R0200, Waltham, MA, USA) were also sorted. Furthermore, the sorting device is placed such, that any movement due to buoyancy is perpendicular to the geometry as shown in Fig. 1.


Fig. 2 The pinched flow fractionation microdevice design. Two separate inlets, for both buffer and sample fluids lead into the pinched segment. The three outlets sort the particles toward multiple outlets for further extraction. All microfluidic channels have a height of 14 μm.

The setup used to analyze the sorting performance has been described previously[20]. In short, the sorting process was imaged using a high-speed camera (Photron, FASTCAM SA-X) connected to a microscope (Olympus, BXFM). The microscope is fitted with one of several objectives: a 60× water-immersion objective (Olympus, LUMPlanFL) was used to measure the $y_b(R)$ curves, a 100× water-immersion objective (Olympus, LUMPlanFL) was used to measure the velocity of microbubbles flowing through the pinched segment, and a 50× long working distance objective (Olympus, SLMPlan) was used to measure the size distributions during sorting. The system was illuminated in bright-field mode using fiber illumination (Olympus ILP-1) connected to a collimation objective (10× Olympus Plan Achromat, 0.25 NA) positioned below the microfluidic chip to maximize the light intensity at the imaging position. The frame rate used was 10,000 frames per second when recording at the outflow positions and 140,000 frames per second when measuring the flow inside the pinched segment. These high frame rates ensured a sufficient time resolution for particle tracking. To minimize motion blur, the exposure time was set to 8 μs during recordings taken at 10,000 frames per second.

Results

Pinched flow fractionation for microbubbles

Figure 3A shows the broadened segment during operation. Separation of the microbubbles by size is clearly observed. The measurement location is positioned 300 μm from the end of the pinched segment. Figure 3B shows the measured positions of 50,000 bubbles as a function of the bubble radius. Some scatter is observed for smaller bubbles, which is due to the following. First, when multiple bubbles travel through the pinched segment in close proximity, bubble-bubble interactions can cause smaller bubbles to be positioned further away from the wall. Second, the finite flow rate ratio sets a lower limit on the size of particles that can be sorted successfully. In Fig.1, the darker blue region indicates the fluid layer consisting of liquid from the sample inlet.

A

B
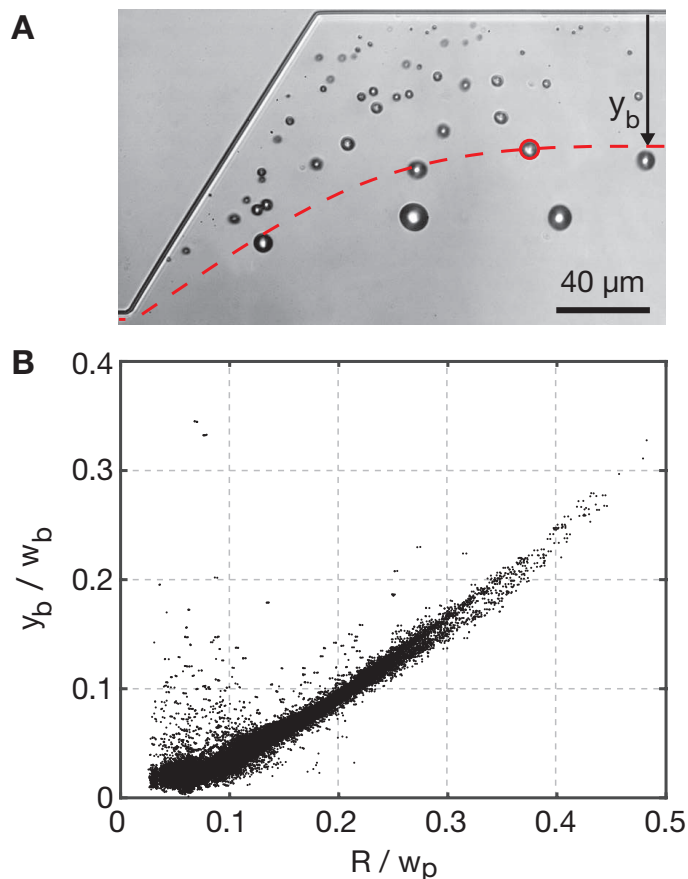
Fig. 3 A) Image obtained from the measurements during the sorting of microbubbles at high concentration (A). To reduce the influence of bubble-bubble interactions, concentrations were kept low during measurements. B) The distance from the wall in the broadened segment y_b as a function of bubble radius R. Successful separation can clearly be observed.

Bubbles smaller than the width of this fluid layer in the pinched segment are not pinned to the wall and as a result they are not sorted[21].

UCA enrichment using pinched flow fractionation

Based on the results as shown in Fig. 3, bubbles with sizes between 1 and 2 μm are expected to enter the center outlet channel. Figure 4 shows the size distributions of the microbubbles entering each of the outlet channels. The data is based on measurements of approximately 22,000 microbubbles, measured during 10 seconds of sorting. The results show successful sorting of the UCA microbubbles, creating a bubble population with a mean radius of 1.56 μm, and a standard deviation of 0.30 μm. Clear bandpass filtering behavior is observed, both bubbles smaller than the target size, and bubbles larger than the target size are excluded from the center outlet.

Sorting quantification

A quantitative comparison of the results as shown in Fig. 3B with the results of the model, Fig. 1B, shows that the distance from the
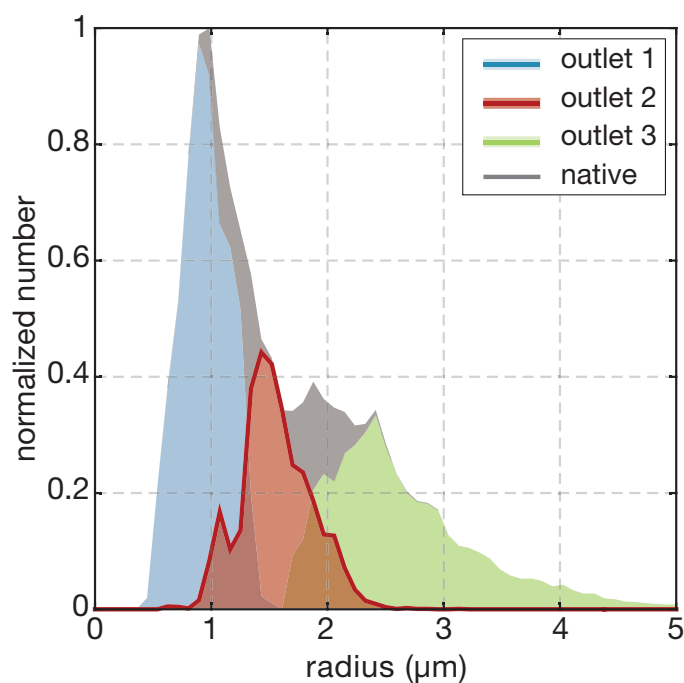
Fig. 4 Size distributions for the microbubbles entering into the three separate outlets. The results show very high selectivity for bubbles of the desired size (in red).

wall in the broadened segment of large bubbles is significantly overestimated by the model, suggesting that the point particle approximation may fail for larger particles. The finite size of the particles influences the flow both by relative translation and by rotation, caused by the velocity gradient.

To investigate this behavior, we determine the flow profile within the pinched segment, with a rotating and translating particle present, from 3D simulations using the COMSOL Multiphysics package[27]. This flow profile is then direct input to Eq. 1 to determine the position in the broadened segment, $y_b(R)$.

The simulation used for the model including the rotation is implemented as a steady-state simulation of the flow in a square cross-section microchannel. A sphere with an imposed translation velocity and rotation rate simulates the presence of the bubble. Due to the coating of the microbubbles, a no-slip boundary condition applies[28]. The velocity vector v_b as function of position on the bubble surface can then be calculated as follows:

$$v_b = (v_p - \Omega R sin(\phi_1) sin(\phi_2))\hat{x} + (\Omega R cos(\phi_1) sin(\phi_2))\hat{y}$$

With v_p the translational velocity of the particle, Ω the rotation rate, and ϕ_1 and ϕ_2 the azimuthal and polar angles, respectively. The translational velocity of the bubbles, which is size-dependent, is determined from high speed measurements of bubbles as they flow through the pinched segment. The rotation rate of the particle is treated as a free parameter, since it cannot be obtained directly from the measurements.

Figure 5A shows the measured velocities, v_p, of the bubbles as they travel through the pinched segment, normalized by the average flow velocity, $\bar{u}$. A series of velocities was found, with the

velocity increasing with size. Based on the measurements of the bubble velocities, maximum and minimum values were obtained for use in the simulations, indicated by the red and blue lines. Figure 5B shows the flow profiles obtained from the simulations for a number of cases, with and without particles, translating and rotating. The resulting position as a function of size and dimensionless rotation rate, defined as $\widetilde{\Omega} \equiv \Omega R / v_p$, is then shown in Fig. 5C.

The results show that the rotation of the particle significantly modifies the flow profile in the pinched segment, causing the effluent position of the particle to lie closer to the wall in the broadened segment. Merely adding a translating, non-rotating, particle to the simulation does not change the outcome significantly. The results obtained for $\widetilde{\Omega} = 0.75$ show good agreement with the measured data. This value of the dimensionless rotation rate is similar to results obtained previously in a numerical study[29]. Figure 5D shows the results of the model for $\widetilde{\Omega} = 0.75$, using the minimum and maximum velocities as indicated in Fig. 5A. Thus, the range of velocities does not significantly change the sorting position.

Discussion

Pinched flow fractionation has many promising advantages as a method for enriching UCAs. The absence of external forcing significantly simplifies device design and the absence of flow rate dependency, as shown here, leads to high repeatability, even when used by general medical practitioners. These characteristics, combined with the simple geometries involved, allow for direct integration with medical syringes, allowing for a point-of-care device capable of producing monodisperse UCA wherever needed, at low cost.

A typical dose of ultrasound contrast agent consists of several billion microbubbles. Injecting an enriched bubble population may decrease the need for such a high volume, a decrease of a factor of 20-40 is expected. However, with only a single sorting channel, as reported in this study, it would still take tens of hours for a single dose, at a sorting rate of about 500 bubbles per second per channel. As mentioned before, sorting devices based on pinched flow fractionation have a simple design, which positions them ideally for parallelization. One thousand parallel channels would already decrease the sorting time to two minutes. This should fit comfortably within a device with a volume of one cubic centimeter, capable of being attached to standard syringes. The low cost of individual units would allow for a single-use device design, which is highly preferable in medical environments due to sterility requirements.

There are several points to be addressed concerning the modelling of the bubble sorting. The dimensionless rotation rate was varied between 0 and 1, corresponding to a state of pure translation and of the particle rolling perfectly along the sidewall. Our experimental results fit closely to $\widetilde{\Omega} = 0.75$, in agreement with earlier numerical results[29]. Due to the homogeneous and spherical nature of our particles and bubbles, we were unable to measure the rotation rate in the current setup. A more rigorous physical insight into the rotation problem will be the subject of further studies.

It is implicitly assumed that the deformability of the bubbles does
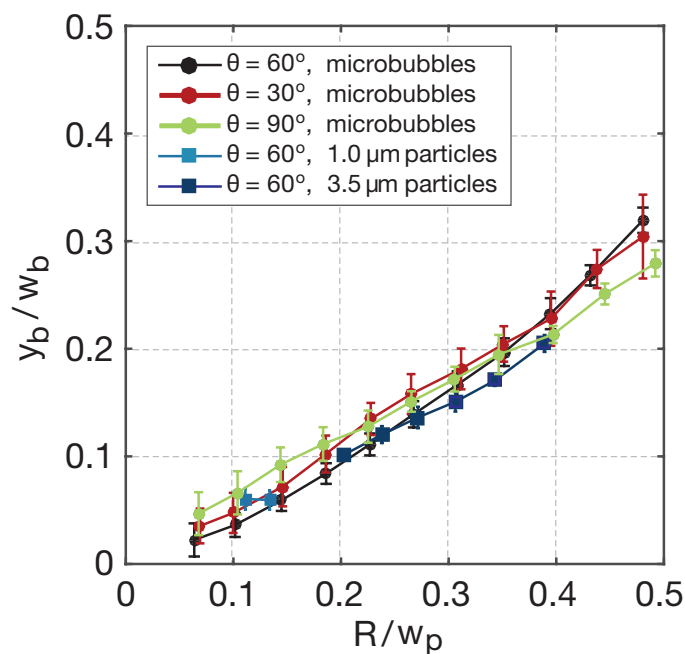
Fig. 6 Comparison of experimental results for varying broadening angle θ, and type of particle used.

not play a role in their sorting behavior. To confirm this, the very same sorting device was used to sort solid particles in the same size range. Figure 6 shows the sorting position as a function of the particle size, for both microbubbles and solid particles. These curves show nearly identical results for microbubbles and solid particles, which therefore excludes any deformability and density effects, in the range of parameters used in this study. We expect that deformation of the microbubbles will become a significant factor for systems an order of magnitude larger.

As stated in the device design parameters, the broadening angle used was $\theta = 60°$. In their pioneering paper, Yamada et al.[21], state that they find an influence of this angle on the sorting behavior. Measurements were performed using devices with broadening angles between 30 and 90°, see Fig. 6. Our results do not show a significant difference between the results for these devices, in the range of flow parameters used in this study.

A possible downside of sorting bubbles by size using pinched flow fractionation with the aim of increasing ultrasound sensitivity, is that the phospholipid packing density in the shell may vary slightly from bubble to bubble. This means that two bubbles of identical size need not necessarily show identical acoustical behavior[30]. This problem is inherent to all sorting methods aimed at sorting by size, and can only be lessened by improving the initial production. To assess the actual gain in sensitivity between unsorted and enriched microbubble populations, we plan to acoustically characterize the enriched population and compare it to the native population.

Conclusions

We have demonstrated a simple lab-on-a-chip device capable of sorting coated microbubbles on-line, using pinched flow fraction-
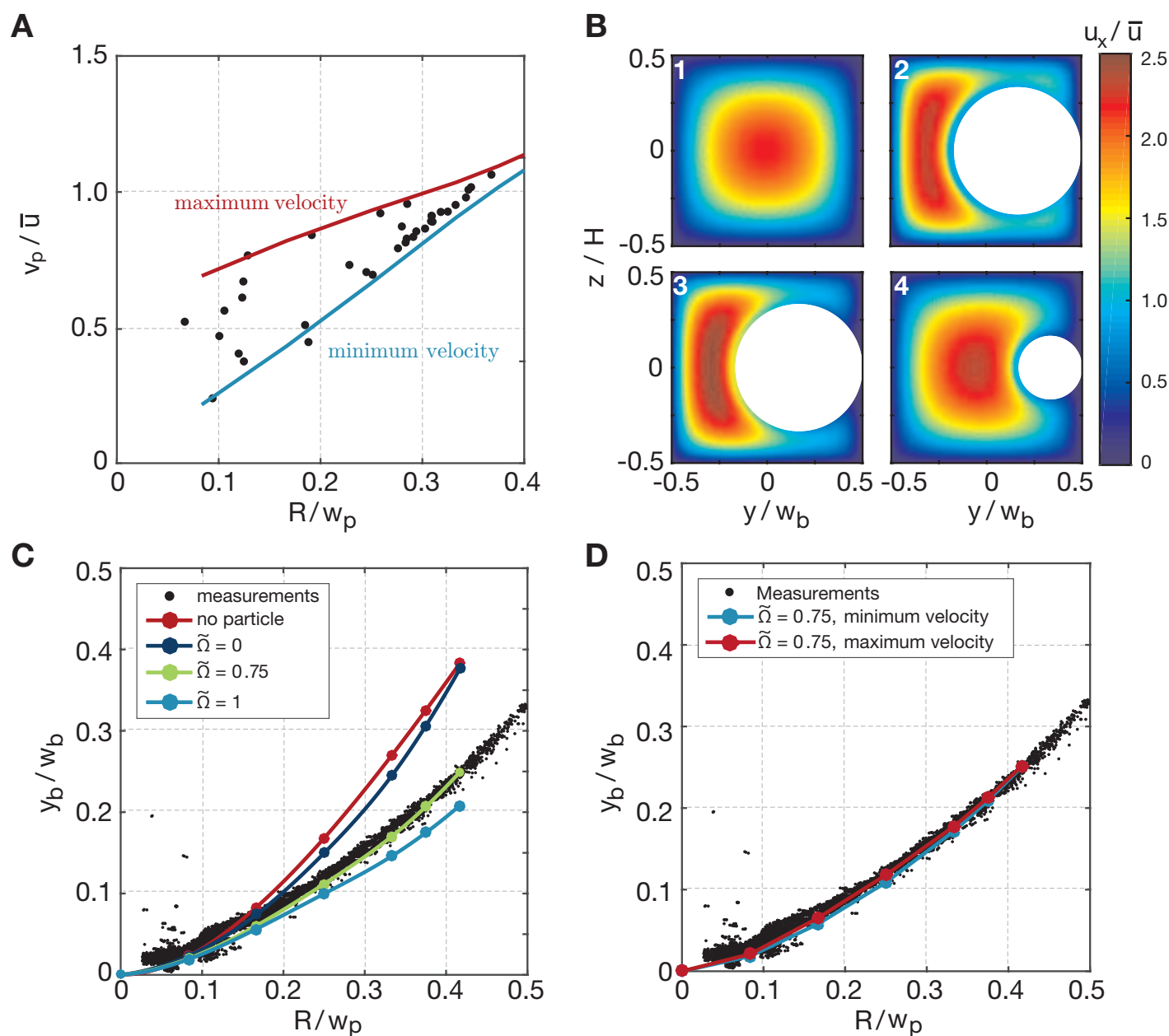
Fig. 5 A) Measured bubble velocities inside the pinched segment as a function of the radius. The lines indicate the maximum and minimum velocities used in the simulations. B) Flow profiles obtained from 3D simulation using COMSOL Multiphysics, using measured velocities as input. B1) The undisturbed flow field, B2) the flow field with a translating but rotationless particle, B3) and B4) the flow field with a particle translating and rotating ($\widetilde{\Omega} = 0.75$), for two different radii. C) The position in the broadened segment as a function of size and dimensionless rotation rate, obtained by using the velocity profiles as direct input into eq. 1. D) Comparison of the numerical results for a value of $\widetilde{\Omega} = 0.75$ for the minimum and maximum velocities to the measured locations.

ation. We have shown that the present models for pinched flow fractionation can be successfully extended to larger particles of the present population, having the same order of size as the pinched segment width, by including particle rotation. Devices based on pinched flow fractionation have simple geometries and flow parameters, which makes them ideally suited for parallelization.

Acknowledgements

References

1 N. de Jong, R. Cornet and C. Lancée, *Ultrasonics*, 1994, **32**, 447.

2 J. R. Lindner, *Nature Reviews Drug Discovery*, 2004, **3**, 527–533.

3 A. L. Klibanov, *Invest. Radiol.*, 2006, **41**, 354–362.

4 J. Tsutsui, F. Xie and R. Porter, *Cardiovasc Ultrasound*, 2004, **2**, 23.

5 S. Hernot and A. L. Klibanov, *Adv. Drug Deliv. Rev.*, 2008, **60**, 1153–1166.

6 L. Deelman, A. Declèves, J. Rychak and K. Sharma, *Adv. Drug Deliv. Rev.*, 2010, **62**, 1369–1377.

7 A. Carson, C. McTiernan, L. Lavery, M. Grata, X. Leng, J. Wang, X. Chen and F. Villanueva, *Cancer Res.*, 2012, **72**, 6191–6199.

8 H. Dewitte, K. Vanderperren, H. Haers, E. Stock, L. Duchateau, M. Hesta, J. Saunders, S. De Smedt and I. Lentacker, *Theranostics*, 2015, **5**, 97–109.

9 E. Talu, K. Hettiarachchi, S. Zhao, R. L. Powell, A. P. Lee, M. L. Longo and P. A. Dayton, *Mol. Imaging*, 2007, **6**, 384–392.

10 M. Overvelde, V. Garbin, B. Dollet, N. de Jong, D. Lohse and M. Versluis, *Ultrasound Med. Biol.*, 2011, **37**, 1500–1508.

11 K. Hettiarachchi, E. Talu, M. L. Longo, P. A. Dayton and A. P. Lee, *Lab. Chip*, 2007, **7**, 463–468.

12 R. Shih, D. Bardin, T. D. Martz, P. S. Sheeran, P. A. Dayton and A. P. Lee, *Lab. Chip*, 2013, **13**, 4816–4826.

13 E. Talu, K. Hettiarachchi, R. Powell, A. Lee, P. Dayton and M. Longo, *Langmuir*, 2008, **24**, 1745–1749.

14 E. Stride and M. Edirisinghe, *Medical and Biological Engineering & Computing*, 2009, **47**, 883–892.

15 M. Emmer, H. J. Vos, D. E. Goertz, A. van Wamel, M. Versluis and N. de Jong, *Ultrasound Med. Biol.*, 2008, **35**, 102–111.

16 D. E. Goertz, N. de Jong and A. F. W. van der Steen, *Ultrasound Med. Biol.*, 2007, **33**, 1376–1388.

17 J. A. Feshitan, C. C. Chen, J. J. Kwan and M. A. Borden, *J. Coll. Interf. Sci*, 2009, **329**, 316–324.

18 R. Marchington, M. Mazilu, S. Kuriakose, V. Garcés-Chávez, P. Reece, T. Krauss, M. Gu and K. Dholakia, *Opt. Soc. Am.*, 2008, **316**, 3712–3726.

19 D. Chen, W. Li, H. Du and M. Li, *J. Nanosc. and Nanotech.*, 2011, **12**, 3035–3039.

20 T. Segers and M. Versluis, *Lab. Chip*, 2014, **14**, 1705–1714.

21 M. Yamada, M. Nakashima and M. Seki, *Anal. Chem.*, 2004, **76**, 5465–5471.

22 H. Maenaka, M. Yamada, M. Yasuda and M. Seki, *Langmuir*, 2008, **24**, 4405–4410.

23 M. Matsuda, M. Yamada and M. Seki, *Electronics and Communications in Japan*, 2011, **94**, 1–6.

24 K. Andersen, S. Levinsen, W. Svendsen and F. Okkels, *Lab on a Chip*, 2009, **9**, 1638–1639.

25 A. Vig and A. Kristensen, *Appl. Phys. Lett.*, 2004, **93**, 203507.

26 D. C. Duffy, J. C. McDonald, O. J. A. Schueller and G. M. Whitesides, *Anal. Chem.*, 1998, **70**, 211–217.

27 *COMSOL Multiphysics*, http://www.comsol.com/, Accessed: March 20, 2015.

28 V. G. Levich, *Physicochemical Hydrodynamics*, Prentice Hall, Englewood Cliffs, 1962.

29 O. Shardt, S. Mitra and J. Derksen, *Chemical Engineering Science*, 2012, **75**, 106–119.

30 J. Sijl, B. Dollet, M. Overvelde, V. Garbin, T. Rozendal, N. de Jong, D. Lohse and M. Versluis, *J. Acoust. Soc. Am.*, 2010, **128**, 3239–3252.

Lab on a Chip Accepted Manuscript